THE JOURNAL OF BIOLOGICAL CHEMISTRY VOL. 292, NO. 5, pp. 1884–1898, February 3, 2017

Nuclear Localization of Integrin Cytoplasmic Domain-associated Protein-1 (ICAP1) Influences β1 Integrin Activation and Recruits Krev/Interaction Trapped-1 (KRIT1) to the Nucleus*

Received for publication, October 6, 2016, and in revised form, December 12, 2016 Published, JBC Papers in Press, December 21, 2017, DOI 10.1074/jbc.M116.762393

Kyle M. Draheim[‡], **Clotilde Huet-Calderwood**[‡], **Bertrand Simon**[‡], **and David A. Calderwood**[‡§1]

From the [‡]*Department of Pharmacology and the* [§]*Department of Cell Biology, Yale University School of Medicine, New Haven, Connecticut 06520*

Edited by Thomas Söllner

Binding of ICAP1 (integrin cytoplasmic domain-associated protein-1) to the cytoplasmic tails of β1 integrins inhibits integrin activation. ICAP1 also binds to KRIT1 (Krev interaction trapped-1), a protein whose loss of function leads to cerebral cavernous malformation, a cerebrovascular dysplasia occurring in up to 0.5% of the population. We previously showed that KRIT1 functions as a switch for β1 integrin activation by antagonizing ICAP1-mediated inhibition of integrin activation. Here we use overexpression studies, mutagenesis, and flow cytometry to show that ICAP1 contains a functional nuclear localization signal and that nuclear localization impairs the ability of ICAP1 to suppress integrin activation. Moreover, we find that ICAP1 drives the nuclear localization of KRIT1 in a manner dependent upon a direct ICAP1/KRIT1 interaction. Thus, nuclear-cytoplasmic shuttling of ICAP1 influences both integrin activation and KRIT1 localization, presumably impacting nuclear functions of KRIT1.

Integrins are heterodimeric trans-membrane adhesion receptors that transduce signals that control complex cell functions, such as survival, proliferation, tissue formation, and homeostasis (1). Integrin signaling is mediated via interactions between their short cytoplasmic tails and cytoplasmic signaling and scaffolding proteins (2, 3). In addition, binding of proteins to the integrin β tails can induce conformational changes in the integrin extracellular domains that alter integrin affinity for extracellular ligands (4). This "inside-out" signaling mechanism alters the integrin activation state and is a key regulator of cell adhesion, cell spreading, cytoskeletal rearrangement, and adhesion signaling.

Integrin activation is triggered by the direct binding of the band four-point-one, ezrin, radixin, moesin (FERM)[2] domain-containing proteins talin and kindlin to two conserved NP*X*Y motifs in the integrin β cytoplasmic tail (5, 6). Notably, negative regulators that bind the integrin cytoplasmic domain and prevent talin or kindlin binding can counteract talin and kindlin-mediated integrin activation (7, 8). Here we report our investigation of one such negative regulator, integrin cytoplasmic domain-associated protein-1 (ICAP1). ICAP1 is a phosphotyrosine binding (PTB) domain-containing protein that interacts selectively with the β1 integrin cytoplasmic domain through a canonical PTB domain/NP*X*Y amino acid motif interaction and inhibits β1 integrin activation by competing with talin and kindlin for binding to the β1 integrin tail (7, 9).

The other well characterized ICAP1-binding protein is Krev interaction trapped-1 (KRIT1) (10, 11). KRIT1 is a multidomain, 736-amino acid protein containing an N-terminal Nudix domain, three NP*X*(Y/F) motifs, an ankyrin repeat domain, and a FERM domain (12). Notably, loss-of-function (typically nonsense) mutations in KRIT1 are associated with cerebral cavernous malformation (CCM), a common dysplasia of the vasculature (13, 14). CCMs consist of clusters of thin-walled, dilated blood vessels that form mulberry-shaped lesions in the brain (15). CCMs have been reported in up to 0.5% of the population (16) and are strongly associated with hemorrhagic stroke, seizure, epilepsy, and other focal neurological outcomes. CCMs are also caused by loss of function mutations in *CCM2* or *CCM3* genes (17), and the CCM2 protein can form the hub of a multiprotein KRIT1-CCM2-CCM3 complex: the CCM complex (12, 18, 19). Loss of KRIT1, CCM2, or CCM3 proteins is therefore directly associated with focal neurological defects, stroke, and vascular abnormalities.

Although not mutated in CCMs, ICAP1 is linked to the CCM complex through its interaction with KRIT1 (7, 20). ICAP1 binds KRIT1 in a bidentate mode, recognizing two regions: the highly conserved RR region and the first of the three KRIT1 NP*X*(Y/F) motifs (7). Importantly, the same binding site on

* This work was supported by National Institutes of Health Grants R01NS085078 (to D. A. C.) and F32HL127948 (to K. M. D.) and by American Cancer Society Grant 122171-PF-12-051-01-CSM (to K. M. D.). The authors declare that they have no conflicts of interest with the contents of this article. The content is solely the responsibility of the authors and does not necessarily represent the official views of the National Institutes of Health.

[1] To whom correspondence should be addressed: Dept. of Pharmacology and of Cell Biology, Yale University School of Medicine, P.O. Box 208066, 333 Cedar St., New Haven, CT 06520-8066. Tel.: 203-737-2311; Fax: 203-785-7670; E-mail: david.calderwood@yale.edu.

[2] The abbreviations used are: FERM, four-point-one, ezrin, radixin, moesin; PTB, phosphotyrosine binding; CCM, cerebral cavernous malformation; NLS, nuclear localization signal(s); NES, nuclear export signal; shSCR, scrambled shRNA; MFI, mean fluorescence intensity; AI, activation index; ANOVA, analysis of variance.

ICAP1 is used to interact with either KRIT1 or integrin β1. By binding ICAP1, KRIT1 inhibits ICAP1 binding to integrins, relieving ICAP1-mediated suppression of integrin activation (7). Consistent with this, increased integrin activation is observed when increasing amounts of KRIT1 are available to bind to ICAP1 (7). In endothelial cells, KRIT1 also appears to stabilize the ICAP1 protein, so KRIT1 loss leads to decreased ICAP1 levels and consequently increased β1 integrin activation (20). In addition to its role with ICAP1, KRIT1 has also been linked to several other important signaling pathways, including Rho/ROCK (21–23), Notch/PI3K (24), reactive oxygen species/SOD2/AKT (25), and β-catenin (26).

ICAP1 and KRIT1 shuttle between the nucleus and cytoplasm, and putative nuclear localization signals (NLS) have been identified in both proteins (27–29). However, very little is understood about shuttling dynamics or its cellular significance. One hypothesis is that KRIT1 and ICAP1 regulate each other by sequestering the partner inside the nucleus, thus preventing interaction with cytoplasmic or membrane proteins, such as β1 integrin (30), but nuclear roles for KRIT1 and ICAP1 are also possible (27, 31). Here we report that ICAP1 contains a functional NLS, which is necessary and sufficient for localization to the nucleus. Deletion or mutation of the ICAP1 NLS prevents nuclear localization, and cytoplasmic ICAP1 is more effective at suppressing the activation of integrin β1. Notably, in co-expression studies, we also find that, by binding KRIT1, ICAP1 drives KRIT1 localization to the nucleus. Thus, nuclear-cytoplasmic shuttling of ICAP1 can influence both integrin activation and KRIT1 localization, presumably influencing the nuclear functions of KRIT1.

Results

The Integrin-binding PTB Domain of ICAP1 Is More Effective Than Full-length ICAP1 at Suppressing β1 Integrin Activation—Consistent with the role of ICAP1 as a direct inhibitor of β1 integrin activation (32–35), we previously demonstrated that expression of green fluorescent protein (GFP)-tagged ICAP1 PTB domain (ICAP1 residues 49–200, $ICAP1_{PTB}$) suppresses β1 integrin activation and that this requires the formation of a typical PTB domain-ligand interaction between integrin β1 and ICAP1 (7). However, ICAP1 contains an additional 48 residues N-terminal to the PTB domain (Fig. 1*A*), and here we investigated whether this region modulates ICAP1-mediated suppression of integrins. We accomplished this by expressing GFP, GFP-tagged full-length ICAP1 (GFP-$ICAP_{FL}$), or GFP-$ICAP1_{PTB}$ constructs in CHO-α5β1 cells and assessing integrin activation using a well validated flow cytometric assay (36). CHO-α5β1 cells are Chinese hamster ovary (CHO) cells that stably express chimeric αIIbα5β3β1 integrins. These integrins contain the cytoplasmic domains of α5β1 and thus are regulated like normal β1 integrins (37) but have the extracellular and transmembrane domains of αIIbβ3. This allowed us to assess activation by measuring binding of the ligand-mimetic anti-αIIbβ3 antibody PAC1 (36). PAC1 binding was normalized to surface integrin expression using an anti-αIIbβ3 integrin antibody that binds in an activation-independent manner, and cells were gated to have comparable GFP intensities. As shown in Fig. 1*B*, we validated the assay by showing that

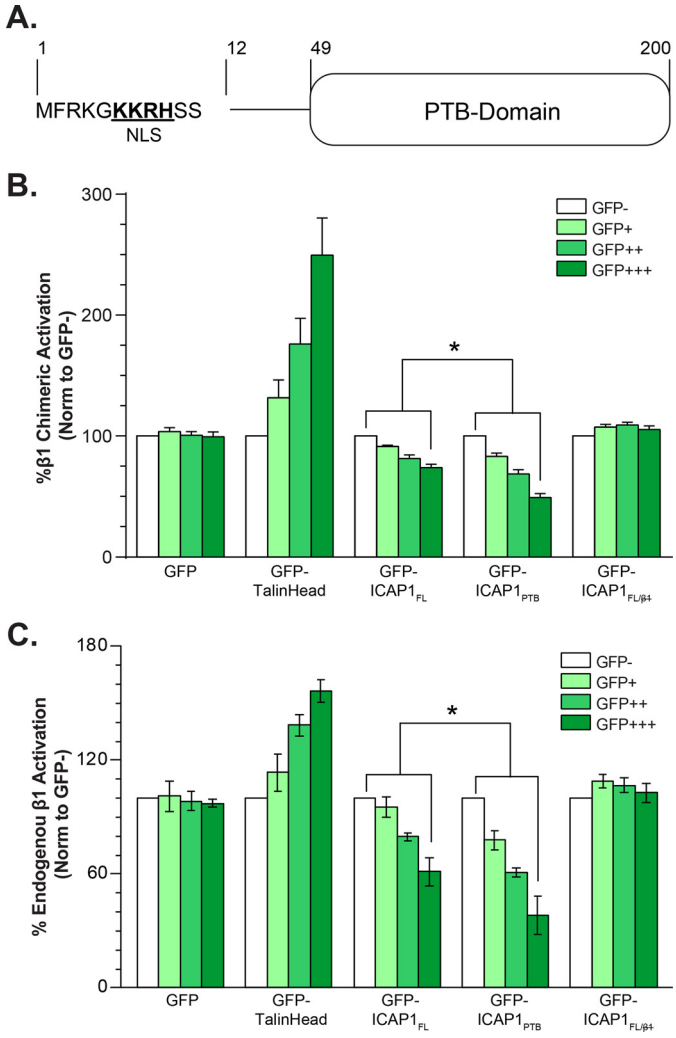

FIGURE 1. **$ICAP1_{FL}$ is less efficient than $ICAP1_{PTB}$ at repressing β1 integrin activation in CHO cells.** *A*, schematic of ICAP1 noting the NLS sequence and PTB-domain boundaries. *B* and *C*, CHO-α5β1 cells (*B*) or CHO cells (*C*) were transfected with GFP, GFP-$ICAP1_{FL}$, GFP-$ICAP1_{PTB}$, the integrin binding-defective mutant GFP-$ICAP1_{FL/β1-}$, or GFP-talin head, and the activation of stably expressed chimeric αIIbα5β3β1 (*B*) or endogenous α5β1 (*C*) integrins was assessed by flow cytometry. Gating on cell populations with different GFP intensities permits analysis of dose-dependent effects. The activation index of each gated population was expressed as the percentage of that in the GFP-negative population. Results are presented as mean percentage ± S.E. (*error bars*) of the activation index in the untransfected (GFP−) population from 4–8 independent experiments. *, $p \leq 0.01$ as determined by a two-way ANOVA with Tukey's correction for multiple tests.

increasing expression of the GFP-tagged integrin activator talin head (5) increased β1 integrin activation, whereas GFP-$ICAP1_{PTB}$ produced a dose-dependent suppression of activation, as reported previously (7). Notably, although GFP-$ICAP1_{FL}$ also triggered dose-dependent inhibition of activation, it was less effective at repressing integrin β1 activation than GFP-$ICAP1_{PTB}$ (Fig. 1*B*). As expected, the ability of $ICAP1_{FL}$ to influence integrin activation depended on an intact β1-binding site because the integrin-binding defective ICAP1 mutant (ICAP1 L135A/I138A/I139A, $ICAP1_{FL/β1-}$) (7) had no impact on integrin activation (Fig. 1*A*).

We have previously shown that the ICAP1 PTB domain regulates chimeric αIIbα5β3β1 integrins in the same way as endogenous α5β1 integrins (7). However, to validate the results

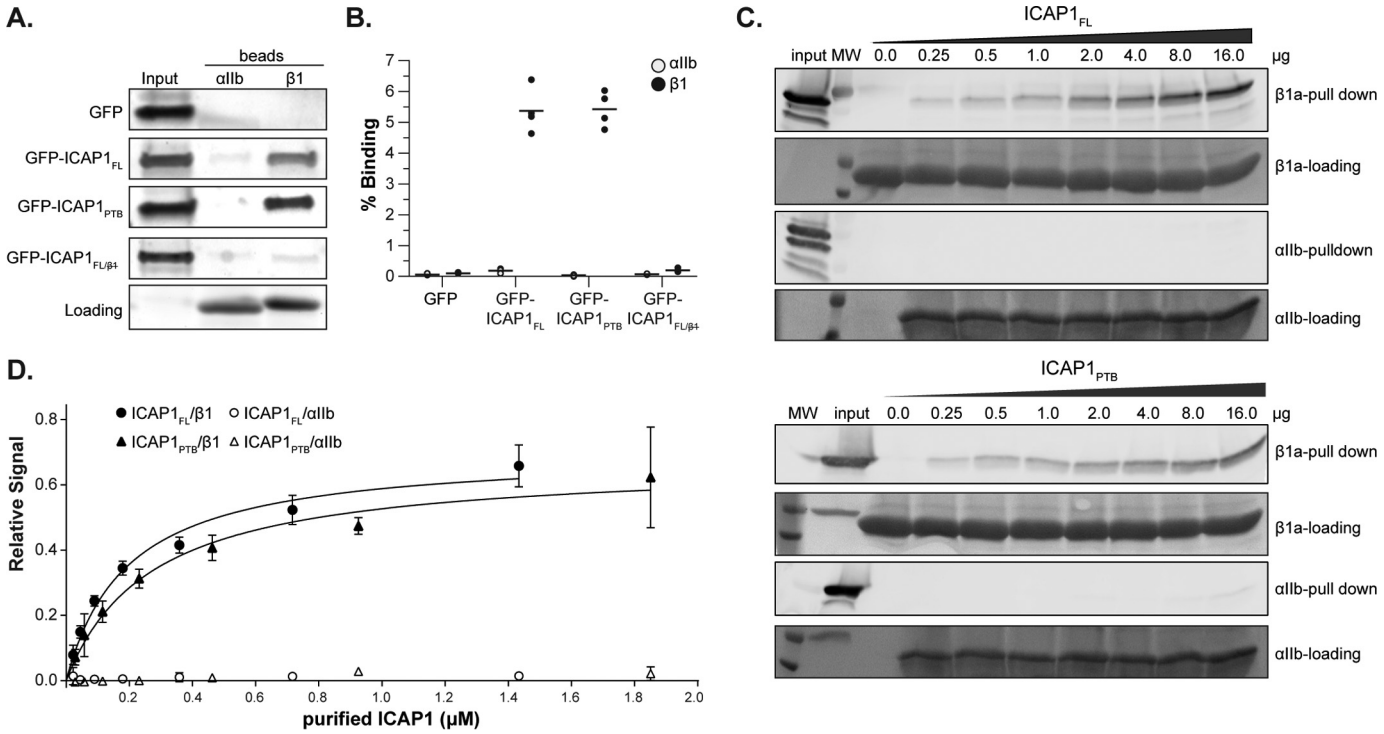

FIGURE 2. **$ICAP1_{FL}$ and $ICAP1_{PTB}$ bind integrin $\beta1$ tails equally well.** *A*, pull-down of GFP-tagged ICAP1 constructs from CHO cell lysates with purified recombinant αIIb or $\beta1$ integrin tails. Tail loading was assessed by Coomassie Blue staining. The *input lane* indicates 5% of input lysate. *B*, ICAP1 binding to purified recombinant αIIb and $\beta1$ tails was quantified and expressed as a percentage of input (mean ± S.E. (*error bars*); $n = 4$). *C*, increasing amounts of purified $ICAP1_{FL}$ or $ICAP1_{PTB}$ were pulled down with His-tagged integrin tails (either αIIb or $\beta1$a) immobilized on beads. Protein was detected by immunoblot analysis. *D*, a binding curve was generated by quantifying the bands, normalizing to the input control, and plotting the relative signal *versus* the input of purified protein (mean ± S.D. (*error bars*), $n = 3$).

in Fig. 1*B*, we also assessed the effect of ICAP1 and ICAP1 mutants on the activation of endogenous CHO cell $\alpha5\beta1$ using a recombinant fragment of fibronectin as a reporter (36). With endogenous integrin (Fig. 1*C*), we obtained results very similar to those with chimeric integrins (Fig. 1*B*), and notably again full-length ICAP1 produced significantly less inhibition of integrin activation than did the ICAP1 PTB domain.

The preceding data indicate that the N-terminal portion of ICAP1 reduces the ability of the ICAP1 PTB domain to suppress integrin activation. It has been suggested that ICAP1 can adopt a closed conformation where the N-terminal and C-terminal portions of the protein associate, masking the integrin-binding site in the ICAP1 PTB domain (38). Deletion of the ICAP1 N-terminal region might disrupt the inhibitory closed conformation, resulting in increased integrin binding, and this could explain why the $ICAP1_{PTB}$ is a more potent inhibitor of $\beta1$ integrin activation than $ICAP1_{FL}$. To test this hypothesis, we compared $ICAP1_{FL}$ and $ICAP1_{PTB}$ binding to integrin $\beta1$. However, pull-down binding assays using cell lysates expressing GFP-ICAP1 constructs and recombinant His-tagged integrin cytoplasmic tails immobilized on beads (39) indicated that there are no major differences between the relative binding of $ICAP1_{FL}$ and $ICAP1_{PTB}$ to integrin $\beta1$ tails (Fig. 2, *A* and *B*). The αIIb beads served to control for background binding. As expected, $ICAP1_{FL/\beta1}$ did not bind to $\beta1$ tails. Our data therefore suggest that deletion of the N terminus of ICAP1 does not alter integrin binding, but to further explore this question, binding curves were determined by incubating increasing amounts of purified recombinant ICAP1 (either FL or PTB) with constant levels of immobilized integrin tails. Beads were washed, and the amount of ICAP1 bound was determined by immunoblot analysis (Fig. 2*C*). The bands were quantified, and curve-fitting analysis demonstrated no significant increase in $ICAP1_{PTB}$ affinity for integrin $\beta1$ tail compared with $ICAP1_{FL}$ (Fig. 2*D*). The 95% confidence interval of K_D for $ICAP1_{PTB}$-$\beta1$ was 0.17–0.44 μM compared with 0.12–0.31 μM for $ICAP1_{FL}$-$\beta1$. These data establish that $ICAP1_{FL}$ retains integrin-binding activity that can be disrupted by mutations in the PTB domain. They further suggest that the N-terminal portion of ICAP1 influences ICAP1-mediated suppression of integrin activation in ways other than directly altering integrin binding affinity.

GFP-$ICAP1_{FL}$ and GFP-$ICAP1_{PTB}$ Show Differential Localization to the Nucleus—To investigate potential mechanisms by which the N-terminal region of ICAP1 might regulate ICAP1 function, we compared the subcellular localization of GFP-$ICAP1_{FL}$ and GFP-$ICAP1_{PTB}$. CHO cells were transfected with either GFP or GFP-tagged ICAP1, plated on fibronectin-coated coverslips, fixed, stained with DAPI (to identify the nucleus), and examined by fluorescence microscopy. It was immediately apparent that GFP-$ICAP1_{FL}$ and GFP-$ICAP1_{PTB}$ differ in their localization to the nucleus (Fig. 3*A*). Whereas GFP exhibited a fairly even distribution between the nucleus and the cytoplasm, and GFP-$ICAP1_{PTB}$ had a similar or perhaps more cytoplasmic distribution, GFP-$ICAP_{FL}$ was strongly enriched in the nucleus, leaving very little GFP-$ICAP1_{FL}$ in the cytosol. Analysis of multiple images from replicate experiments using CellProfiler version 2.0 (40) allowed us to calculate the relative intensity of the GFP signal co-localizing with the nucleus (identified using the

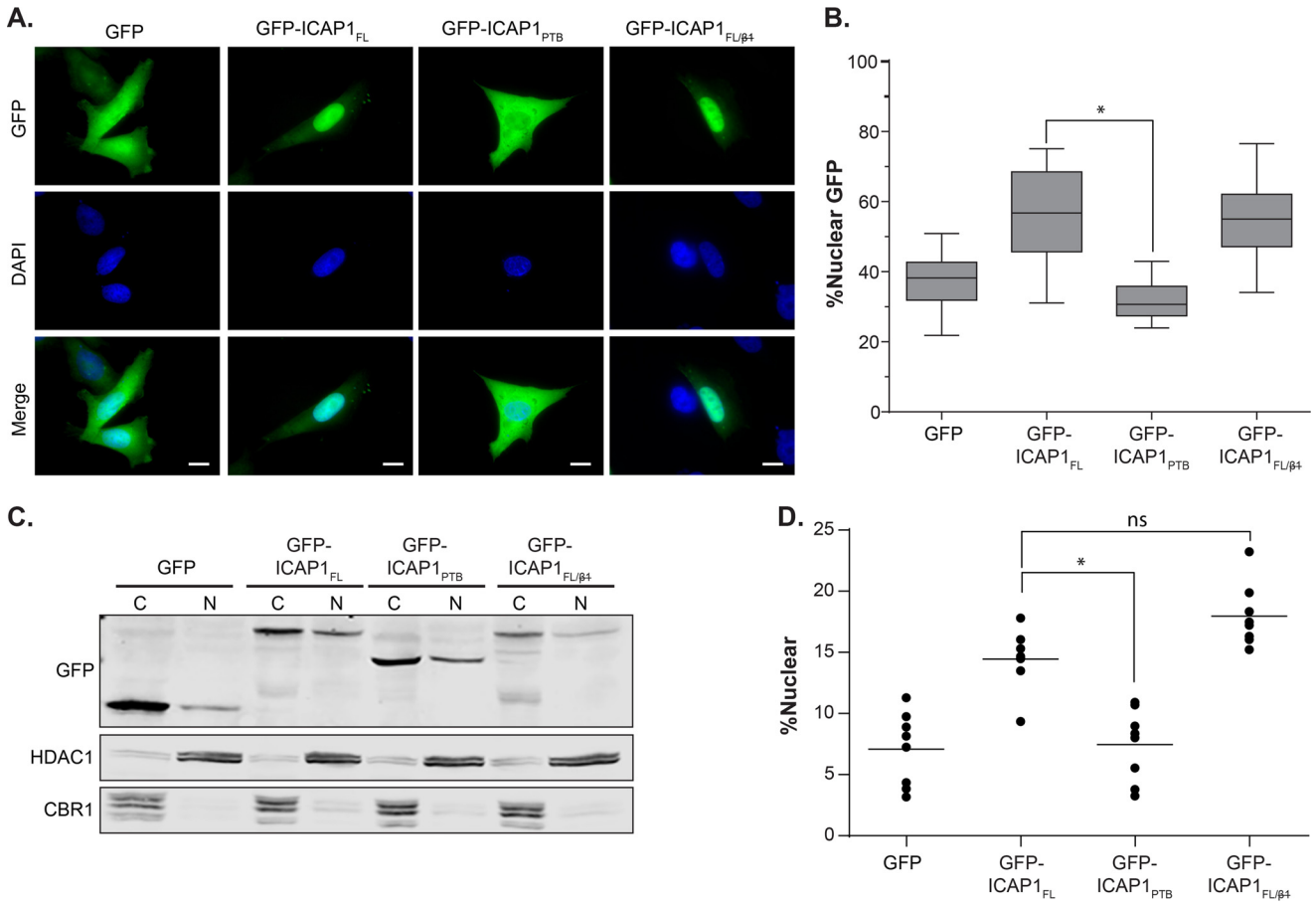

FIGURE 3. **$ICAP1_{FL}$ is more nuclear than $ICAP1_{PTB}$.** *A*, CHO cells overexpressing GFP-tagged ICAP1 constructs were plated on fibronectin, fixed 24 h later, and stained with DAPI to identify nuclei. Representative images are shown; *bar*, 10 μm. *B*, percentage of GFP intensity in the nucleus compared with the integrated GFP intensity of the entire cell was calculated using CellProfiler version 2.0. *Boxes*, 25th through 50th and 50th through 75th percentile; *whiskers*, 5th through 95th percentile ($n = 97–130$ cells from 5 independent experiments). *, $p \leq 0.0001$ as determined by a one-way ANOVA with Tukey's correction for multiple tests. *C*, representative fractionation of CHO cells overexpressing GFP-tagged ICAP1 constructs. *C*, 28% of the cytoplasmic fraction; *N*, 80% of the nuclear fraction. Carbonyl reductase (*CBR1*) and histone deacetylase (*HDAC1*) represent quality controls for cytoplasmic and nuclear fractions, respectively. *D*, quantification of cell fractionation data, where the percentage nuclear = total nuclear/(total nuclear *N* + total cytoplasmic) × 100 (*bar*, mean percentage nuclear value; $n = 10$). *, $p \leq 0.001$ as determined by a one-way ANOVA with Tukey's correction for multiple tests.

DAPI stain) *versus* the whole cell. When quantified, ~56% of the GFP-$ICAP1_{FL}$ signal was nuclear, whereas GFP-$ICAP1_{PTB}$ was statistically significantly lower with ~32% of the signal nuclear (Fig. 3*B*). To validate our image-based findings using a biochemical assay, CHO cells infected by lentivirus to stably express GFP or GFP-tagged ICAP1 constructs were fractionated into nuclear and cytoplasmic fractions and analyzed by immunoblotting (28% of the cytoplasmic fractions and 80.0% of the nuclear fractions were loaded on the gel). Markers of nucleus (HDAC-1) and cytosol (carbonyl reductase) were used to verify the purity of nuclear and cytoplasmic fractions. Consistent with our microscopy data, a greater percentage of $ICAP1_{FL}$ than $ICAP1_{PTB}$ was found in the nuclear fraction (Fig. 3*C*). When quantified across multiple independent replicates, these differences were statistically significant (Fig. 3*D*). We do note that, as observed by other investigators (27, 41, 42), percentages of nuclear ICAP1 measured by fractionation were lower than those obtained by quantitative fluorescence microscopy. Nonetheless, both fluorescence microscopy and cell fractionation indicated that $ICAP1_{FL}$ is more nuclear than the $ICAP1_{PTB}$ domain.

Preferential localization of GFP-$ICAP1_{FL}$ in the nucleus, away from β1 integrins, provides a potential mechanism for the reduced ability of $ICAP1_{FL}$ to suppress β1 activation. Loss of β1 binding had little effect on ICAP1 localization (Fig. 3, *B* and *D*). Collectively, our data indicate that enhanced suppression of β1 activation correlates with decreased nuclear targeting of ICAP1.

ICAP1 Contains a Functional N-terminal Nuclear Localization Signal—ICAP1 is a relatively small protein (200 amino acids) with a known C-terminal PTB domain and an N terminus that is predicted to be unstructured (Fig. 1*A*). ICAP1 has previously been shown to shuttle in and out of the nucleus, and a putative N-terminal NLS was identified (27). Because this sequence is outside of the PTB domain, this would explain why the PTB domain alone has a localization different from that of the full-length protein. To explore the role of this sequence in ICAP1 localization, we generated three GFP-tagged ICAP1 constructs: a truncation of the first 17 amino acids removing the putative NLS (ICAP1 residues 18–200, $ICAP1_{\Delta NLS}$), a mutation of NLS lysine residues to alanine (ICAP1 K6A/K7A, $ICAP1_{NLSmut}$), and the introduction of a premature stop codon

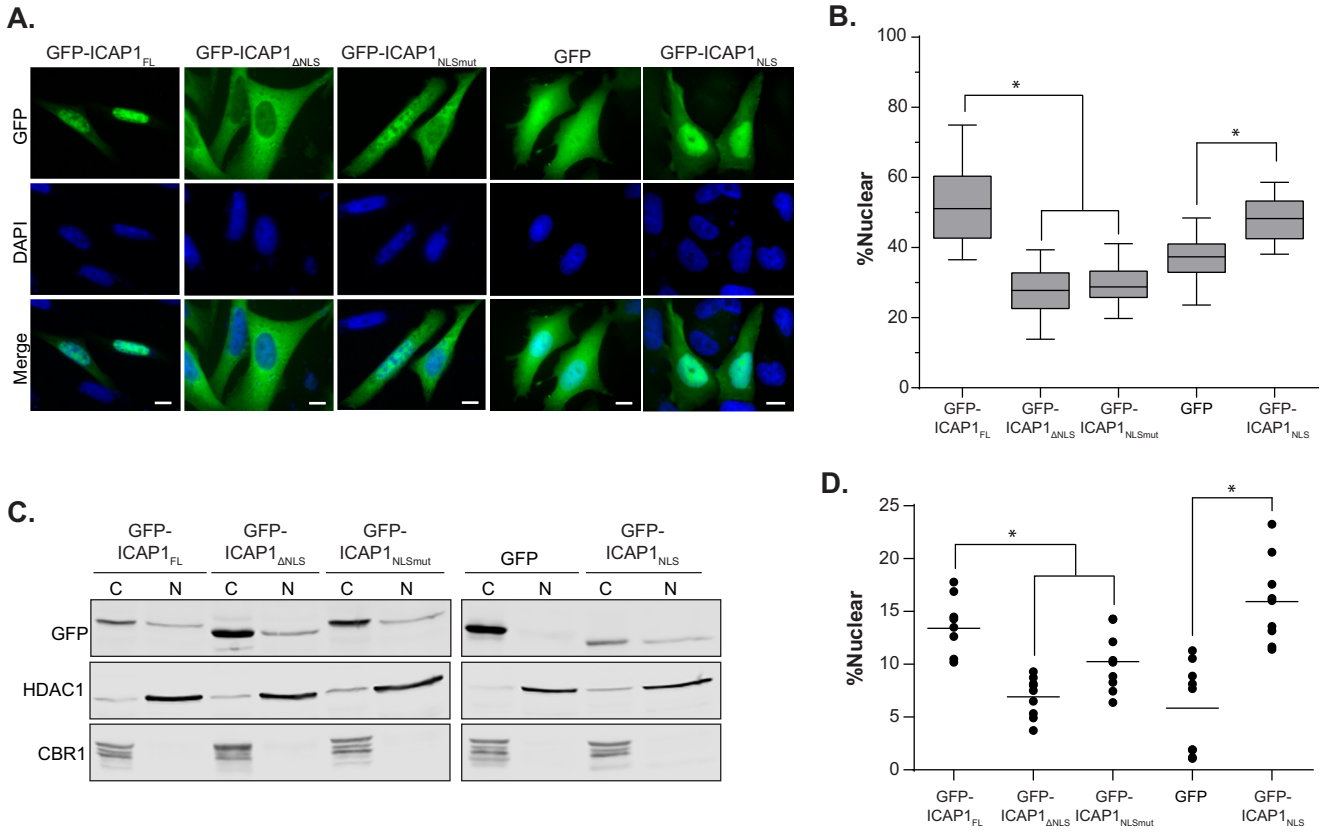

FIGURE 4. **ICAP1 contains a functional NLS.** *A*, CHO cells overexpressing GFP-tagged ICAP1 constructs were plated on fibronectin, fixed 24 h later, and stained with DAPI to identify nuclei. Representative images are shown; *bar*, 10 μm. *B*, relative amount of GFP intensity in the nucleus compared with the integrated GFP intensity of the entire cell. *Boxes*, 25th through 50th and 50th through 75th percentile; *whiskers*, 5th through 95th percentile (n = 88–139 cells from 5 independent experiments). *, $p \leq 0.005$ as determined by a one-way ANOVA with Tukey's correction for multiple tests. *C*, representative fractionation of CHO cells overexpressing GFP-tagged ICAP1 constructs. *C*, 28% of the cytoplasmic fraction; *N*, 80.0% of the nuclear fraction. Carbonyl reductase (*CBR1*) and histone deacetylase (*HDAC1*) represent quality controls for cytoplasmic and nuclear fractions, respectively. *D*, quantification of cell fractionation data where the percentage nuclear = total nuclear/(total nuclear *N* + total cytoplasmic) × 100 (*bar*, mean percentage nuclear value; n = 9). *, $p \leq 0.02$ as determined by a one-way ANOVA with Tukey's correction for multiple tests.

after the NLS (ICAP1 residues 1–10, $ICAP1_{NLS}$). After transfection into CHO cells and plating on FN-coated coverslips, the cellular localization of GFP-ICAP1 was analyzed using fluorescence microscopy. Whereas GFP-$ICAP1_{FL}$ preferentially targeted to the nucleus, both GFP-$ICAP1_{\Delta NLS}$ and GFP-$ICAP1_{NLSmut}$ demonstrated a clear shift to the cytoplasm, exhibiting less nuclear localization than control GFP (Fig. 4*A*). These data demonstrate that the ICAP1 NLS is necessary for nuclear localization, and they are consistent with prior analyses (27). Additionally, we showed that the first 10 amino acids of ICAP1, which contain the $ICAP1_{NLS}$, are sufficient to strongly localize GFP to the nucleus (Fig. 4*A*). Quantification of multiple images revealed that disrupting the NLS sequence by either truncation or mutation causes a statistically significant reduction of nuclear ICAP1, whereas the addition of the ICAP1 NLS to GFP significantly increases localization of GFP to the nucleus (Fig. 4*B*). Again, we validated our findings biochemically by fractionating CHO lines that stably express GFP or GFP-tagged ICAP1 constructs (Fig. 4, *C* and *D*). Collectively, these data suggest that the ICAP1 NLS is both necessary and sufficient for nuclear localization.

Disrupting ICAP1 Nuclear Localization Enhances Suppression of β1 Integrin—To test whether altering ICAP1 localization to the nucleus influences its ability to suppress integrin activation, we transiently expressed GFP-ICAP1 mutants in CHO-$\alpha5\beta1$ cells and assessed $\beta1$ integrin activation using our flow cytometric assay. Notably, whereas $ICAP1_{FL}$, $ICAP1_{\Delta NLS}$, and $ICAP1_{NLSmut}$ each produced dose-dependent suppression of integrin activation, ICAP1 with a disrupted NLS ($ICAP1_{\Delta NLS}$ and $ICAP1_{NLSmut}$) exhibited a significantly greater suppression of integrin $\beta1$ activation (Fig. 5*A*). The increased suppression of $\beta1$ integrin cannot be explained by changes in the level of integrin expression because no significant alteration in integrin levels was observed, and PAC1 binding was normalized to surface integrin expression. Differences in ICAP1-mediated $\beta1$ integrin suppression cannot be due to variations in expression of the ICAP1 constructs because populations were gated for equivalent GFP expression levels, ensuring comparison of cells with comparable levels of GFP-ICAP1. Furthermore, both GFP-$ICAP1_{\Delta NLS}$ and GFP-$ICAP1_{NLSmut}$ appeared to bind $\beta1$ cytoplasmic tails to the same extent as GFP-$ICAP1_{FL}$ when assessed in pull-down assays (Fig. 5*B*). As expected, GFP-$ICAP1_{NLS}$, which lacks the integrin-binding PTB domain, did not bind $\beta1$ tails in pull-down assays and did not impact integrin activation (Fig. 5, *A* and *B*). These data suggest the ICAP1 NLS diminishes $\beta1$ suppression by translocating ICAP1 to the nucleus, away from $\beta1$ integrins.

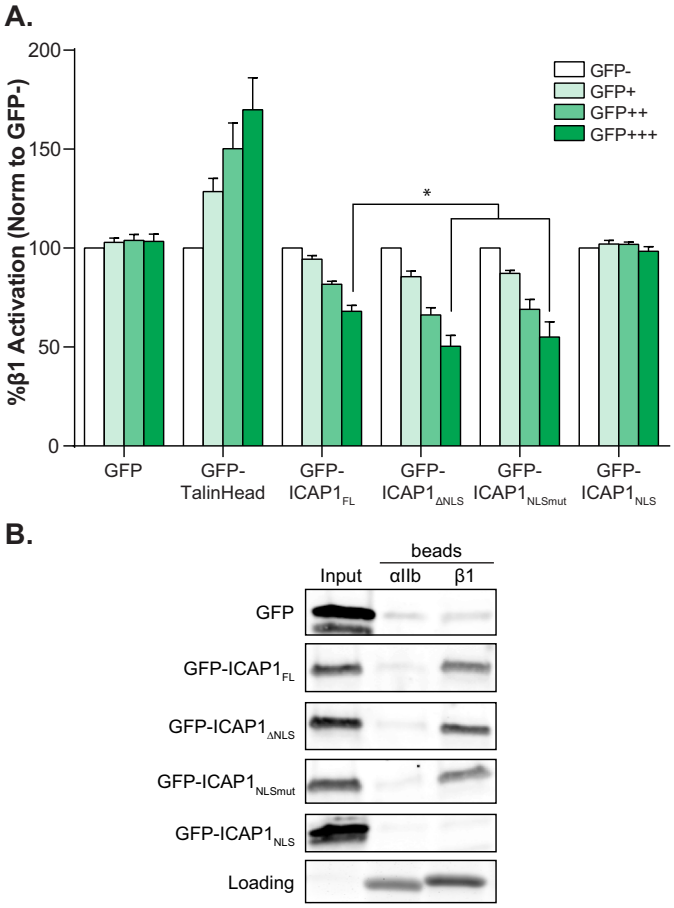

FIGURE 5. **Localization of ICAP1 to the nucleus diminishes its suppression of β1-integrin activation.** *A*, CHO cells were transfected with GFP, GFP-talin head, or GFP-tagged ICAP1 constructs, and the activation of stably expressed chimeric αIIbα5β3β1 integrins was assessed by flow cytometry. Gating on cell populations with different GFP intensities permits analysis of the dose dependence of effects. Results are the mean percentage ± S.E. (*error bars*) of the untransfected (*GFP−*) population from 6–8 independent experiments. *, $p \leq 0.001$ as determined by a two-way ANOVA with Tukey's correction for multiple tests. *B*, pull-down of GFP-tagged ICAP1 constructs from CHO cell lysates with purified recombinant αIIb or β1 integrin tails. Tail loading was assessed by Coomassie Blue staining. The *input lane* indicates 5% of input lysate. Results shown are representative of four independent experiments.

Binding to ICAP1 Drives Nuclear Localization of the N-terminal Fragment of KRIT1—We have shown previously that the N-terminal fragment of KRIT1 (KRIT1 residues 1–198, $KRIT1_{Nterm}$) inhibits ICAP1-mediated suppression of integrin β1 activation by competing with β1 integrin for binding to ICAP1 (7). Additionally, data from other laboratories suggest that KRIT1 localization drives ICAP1 localization (28). To test whether cellular localization might play a role in the reversal of ICAP1-mediated integrin suppression by KRIT1, we co-expressed GFP or GFP-tagged $KRIT1_{Nterm}$ with DsRed or DsRed-tagged ICAP1 in CHO cells and evaluated nuclear localization in double positive cells. As expected, GFP co-expression had little impact on the localization of DsRed-ICAP1 or DsRed-ICAP1 mutants (Fig. 6*A*). DsRed-$ICAP1_{FL}$ exhibited greater nuclear localization than DsRed, whereas DsRed-$ICAP1_{ΔNLS}$ and DsRed-$ICAP1_{NLSmut}$ exhibited less nuclear localization, a pattern very similar to that seen for GFP-tagged proteins in Fig. 4*B*. However, when $KRIT1_{Nterm}$ (which contains the ICAP1-binding site) was expressed, the mean nuclear fraction of DsRed-$ICAP1_{FL}$ statistically significantly increased from 49 to 61% (Fig. 6*A*). Notably, a direct $ICAP1_{FL}$/$KRIT1_{Nterm}$ interaction was required for this increase in nuclear ICAP1, because co-expression of $KRIT1_{Nterm}$ containing mutations that inhibit ICAP1 binding (7) (KRIT1 R179A/R185A/N192A/Y195A, $KRIT1_{Nterm/\cancel{ICAP1}}$) did not have this effect (Fig. 6*A*). These data are consistent with reports that KRIT1 drives ICAP1 nuclear localization (28). However, neither DsRed-$ICAP1_{ΔNLS}$ nor DsRed-$ICAP1_{NLSmut}$ showed any significant changes in localization when co-expressed with either GFP-$KRIT1_{Nterm}$ or GFP-$KRIT1_{Nterm/\cancel{ICAP1}}$ (Fig. 6*A*). Thus, $KRIT1_{Nterm}$ was unable to enhance nuclear targeting of ICAP1 lacking a functional NLS, showing that binding to $KRIT1_{Nterm}$ is insufficient to target ICAP1 to the nucleus.

In the process of assessing the impact of $KRIT1_{Nterm}$ on ICAP1 localization, we noticed that ICAP1 profoundly altered $KRIT1_{Nterm}$ localization. When GFP-$KRIT1_{Nterm}$ was co-expressed with DsRed, GFP-$KRIT1_{Nterm}$ had an even distribution throughout the cell, comparable with the distribution of GFP alone (Fig. 6*B*). However, when co-expressed with DsRed-$ICAP1_{FL}$, which localizes strongly to the nucleus, GFP-$KRIT1_{Nterm}$ localization shifted to the nucleus (Fig. 6*B*). Additionally, when co-expressed with either DsRed-$ICAP1_{ΔNLS}$ or DsRed-$ICAP1_{NLSmut}$, which exhibit more cytoplasmic localization, GFP-$KRIT1_{Nterm}$ also localized more to the cytoplasm (Fig. 6*B*). Thus, GFP-$KRIT1_{Nterm}$ appears to follow the localization of ICAP1, and mutations that alter ICAP1 localization also influence that of KRIT1. The effect of ICAP1 on $KRIT1_{Nterm}$ localization appears to depend on a direct KRIT1-ICAP1 interaction because GFP-$KRIT1_{Nterm/\cancel{ICAP1}}$ localization was not affected by co-expression of any of the DsRed-ICAP1 constructs (Fig. 6*B*). Overall, our data suggest that, whereas binding to the N-terminal portion of KRIT1 enhances nuclear localization of ICAP1, $KRIT1_{Nterm}$ is insufficient to drive ICAP1 localization; instead, ICAP1 drives KRIT1 localization in a binding-dependent manner.

Mutations in KRIT1 Lead to Changes in Cellular Localization—The preceding experiments investigated the role of the N-terminal portion of KRIT1 encompassing the Nudix domain and the first NPXY motif. However, KRIT1 is a multidomain protein that, in addition to having several other binding partners, contains two putative NLS and one predicted nuclear export signal (NES) (Fig. 7*A*) (17, 28, 30, 43, 44). To determine the localization of full-length KRIT1 ($KRIT1_{FL}$) and the role of the predicted NLS and NES in the absence of co-expressed ICAP1, GFP-tagged KRIT1 was overexpressed in CHO cells (which do not express either endogenous ICAP1 or KRIT1 (45)). We generated mutants that disrupted either the NLS1 (KRIT1 K46A/K47A/K48A/R49A/K50A/K51A, $KRIT1_{FL\text{-}NLS1mut}$), NLS2 (KRIT1 K569A/K570A/H571A/K572A, $KRIT1_{FL\text{-}NLS2mut}$), or NES (KRIT1 L557A/L558A/L559A, $KRIT1_{FL\text{-}NESmut}$). $KRIT1_{FL}$ constructs were then expressed in CHO cells by lentiviral transduction. GFP-$KRIT1_{FL}$, like GFP-$KRIT1_{Nterm}$, distributed evenly between the nucleus and the cytoplasm (Fig. 7*B*). Interestingly, only GFP-$KRIT1_{NLS1mut}$ showed a change in localization, whereas the cellular localization of GFP-$KRIT1_{FL\text{-}NESmut}$ and GFP-$KRIT1_{FL\text{-}NLS2mut}$ was indistinguishable from GFP-$KRIT1_{FL}$ (Fig. 7*B*). When quantified, GFP-$KRIT1_{FL\text{-}NLS1mut}$ was statistically less

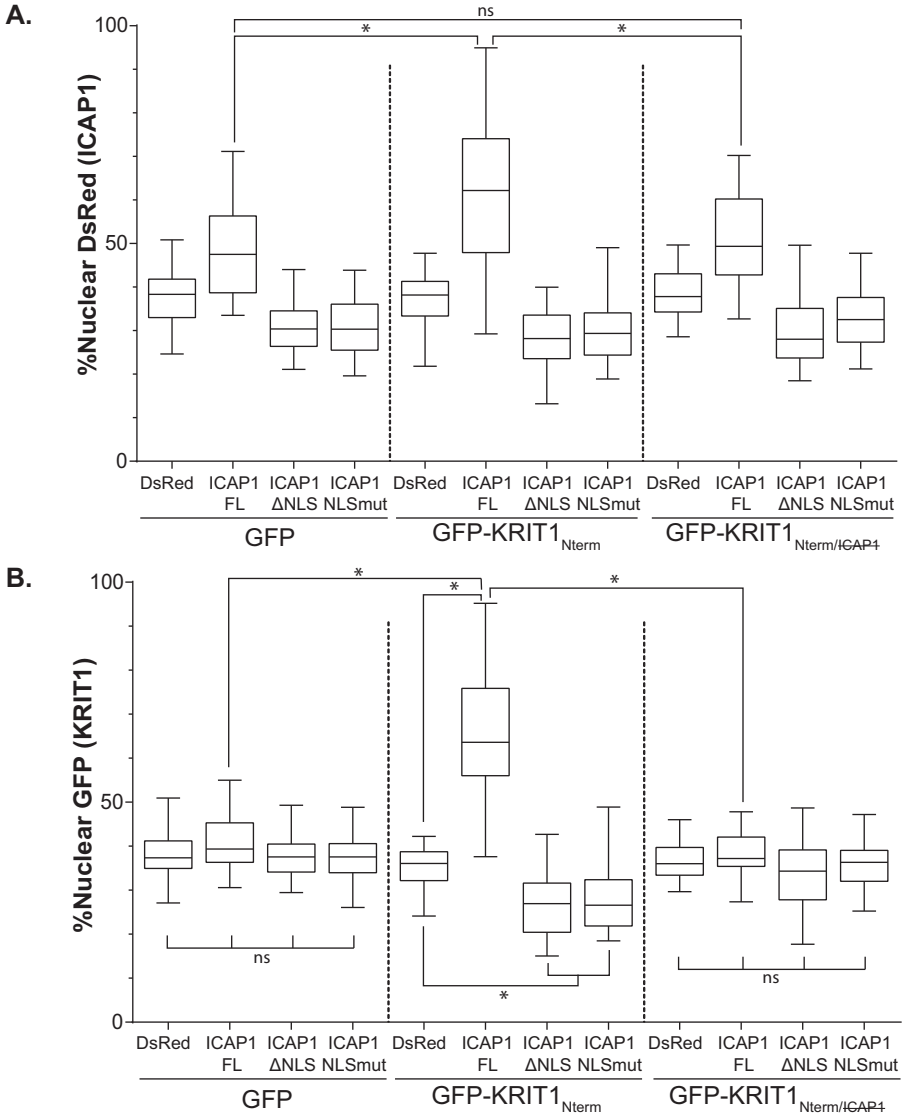

FIGURE 6. **Localization of KRIT1$_{Nterm}$ is driven by ICAP1.** *A* and *B*, CHO cells co-overexpressing GFP-tagged KRIT1 constructs and DsRed-tagged ICAP1 constructs were plated on fibronectin, fixed 24 h later, and stained with DAPI to identify nuclei. Images were analyzed using CellProfiler. Percentage nuclear fluorescence compared with the total integrated fluorescence intensity of the entire cell for DsRed (*A*) and GFP (*B*) was calculated. *Boxes*, 25th through 50th and 50th through 75th percentile; *whiskers*, 5th through 95th percentile ($n = 62–138$ cells from 3 independent experiments). *, $p \leq 0.0001$ as determined by a one-way ANOVA with Tukey's correction for multiple tests.

nuclear than KRIT1$_{FL}$ (24% compared with 35%, respectively), whereas the other mutants showed no change (Fig. 7*B*).

ICAP1 Drives KRIT1$_{FL}$ Localization in a Binding-dependent Fashion—To test whether ICAP1 could drive the localization of KRIT1$_{FL}$, as it did for KRIT1$_{Nterm}$, KRIT1$_{FL}$ constructs were overexpressed in CHO cells by lentiviral transduction, and the ICAP1 constructs were transfected the next day. Double-positive cells were then imaged and analyzed by CellProfiler version 2.0. GFP localization was not affected by ICAP1 expression (Fig. 8*A*), but DsRed-ICAP1$_{FL}$ was able to drive significant nuclear localization of GFP-KRIT1$_{FL}$ (Fig. 8*A*). This result is very similar to that obtained with GFP-KRIT1$_{Nterm}$ (Fig. 6*B*). Furthermore, co-expression of either DsRed-ICAP1$_{\Delta NLS}$ or DsRed-ICAP1$_{NLSmut}$ with KRIT1$_{FL}$ decreased the nuclear fraction of KRIT1$_{FL}$ (Fig. 8*A*). As seen for KRIT1$_{Nterm}$, the ability of ICAP1 to influence KRIT1 localization is dependent on their interaction because the binding-defective GFP-KRIT1$_{FL/\sout{ICAP1}}$ was evenly distributed throughout the cell and was not affected by ICAP1 expression (Fig. 8*A*). To evaluate the contribution of KRIT1 NLS1, the ICAP1 constructs were co-expressed with GFP-KRIT1$_{FL\text{-}NLS1mut}$, a mostly cytoplasmic KRIT1 construct. Most interestingly, the nuclear fraction of GFP-KRIT1$_{FL\text{-}NLS1mut}$ increased when co-expressed with DsRed-ICAP1$_{FL}$, reaching levels comparable with that of KRIT1$_{FL}$ when co-expressed with ICAP1$_{FL}$ (Fig. 8*A*). Together, our data suggest that the ICAP1 NLS is sufficient to take both ICAP1 and KRIT1$_{FL}$ to the nucleus, indicating that ICAP1 drives KRIT1$_{FL}$ localization.

KRIT1 Needs Its NLS1 to Enhance Nuclear Accumulation of ICAP1—We previously noted that although GFP-KRIT1$_{Nterm}$ was insufficient to support ICAP1$_{NLSmut}$ or ICAP1$_{\Delta NLS}$ nuclear localization (Fig. 6*A*), it did nevertheless increase nuclear targeting of DsRed-ICAP1$_{FL}$. We therefore examined the effect of KRIT1$_{FL}$ on ICAP1 localization. As was seen before, GFP did not affect the localization of any of the ICAP1 constructs (Fig.

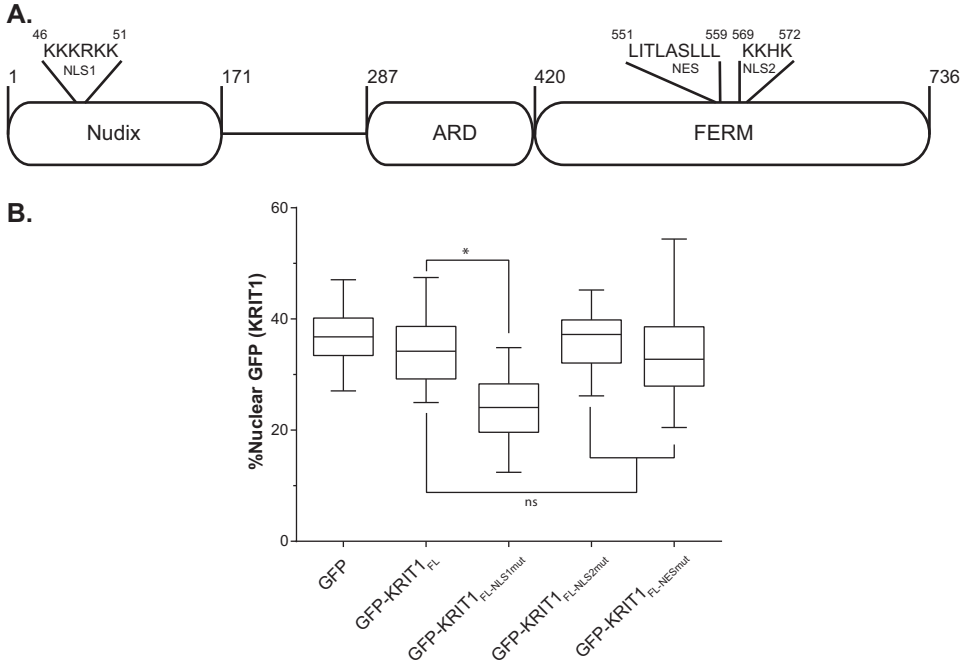

FIGURE 7. **Evaluation of putative KRIT1 localization sequences.** *A*, schematic of KRIT1 noting the sequence of NLS1, NES, and NLS2 as well as domain boundaries. *B*, CHO cells overexpressing GFP-tagged KRIT1 constructs were plated on fibronectin, fixed 24 h later, and stained with DAPI to identify nuclei. Representative images are shown; *bar*, 10 μm. *C*, relative amount of GFP intensity in the nucleus compared with the integrated GFP intensity of the entire cell. *Boxes*, 25th through 50th and 50th through 75th percentile; *whiskers*, 5th through 95th percentile ($n = 85$–157 cells from 4 independent experiments). *, $p \leq 0.0001$ as determined by a one-way ANOVA with Tukey's correction for multiple tests.

8*B*). However, co-expression with GFP-KRIT1$_{FL}$ caused a statistically significant increase of nuclear DsRed-ICAP1$_{FL}$ (46.7% *versus* 56.5%), and this did not occur when DsRed-ICAP1$_{FL}$ was co-expressed with GFP-KRIT1$_{FL/\not ICAP1}$. This validates the earlier finding that the ICAP1/KRIT1 interaction increases nuclear ICAP1. Intriguingly, co-expression of GFP-KRIT1$_{FL\text{-}NLS1mut}$ did not cause an increase in nuclear DsRed-ICAP1$_{FL}$. This suggests that, whereas the ICAP1 NLS is necessary and sufficient for the nuclear localization of the ICAP1-KRIT1 complex and the KRIT1 NLS1 is dispensable for nuclear accumulation of the complex, the NLS1 of KRIT1 is nonetheless required to maintain the highest levels of nuclear ICAP1.

KRIT1$_{FL}$ Localization Changes When Endogenous ICAP1 Is Lost—The preceding experiments all relied on expression of fluorophore-tagged ICAP1 in CHO cells, a line that apparently lacks endogenous ICAP1 and KRIT1 (45). We therefore assessed ICAP1 nuclear localization in EA.hy926 cells, a widely used cell line generated by fusing human umbilical vein endothelial cells with the lung carcinoma A549. EA.hy926 cells retain many endothelial features and can be stably cultured for long periods (46). We have been unable to identify anti-ICAP1 antibodies suitable for immunofluorescence microscopy and therefore used cell fractionation to investigate the nuclear localization of endogenous ICAP1. This revealed that, as observed for exogenously expressed GFP-ICAP1, endogenous ICAP1 is present in both the cytosol and the nucleus (Fig. 9*A*).

Having established that endogenous ICAP1 is found in the nucleus of EA.hy926 cells, we next wished to evaluate how the loss of endogenous ICAP1 affects the localization of KRIT1. Unfortunately, stable knockdown of ICAP1 results in loss of KRIT1 protein (20, 43), preventing us from evaluating the effect of ICAP1 knockdown on endogenous KRIT1 localization. Therefore, we introduced GFP, GFP-KRIT1$_{FL}$, or GFP-KRIT1$_{FL/\not ICAP1}$ into EA.hy926 cells by lentiviral transduction. These cells were then infected with one of two different lentiviral shRNA constructs targeting ICAP1 (shICAP1-21 and shICAP1-23) or a scrambled shRNA (shSCR) control. Cells were treated with puromycin (the shRNA selection marker) and either plated on FN-coated coverslips for fluorescence microscopy or lysed for immunoblot analysis to assess knockdown. As shown in Fig. 9*B*, shICAP1-21 and shICAP1-23 both reduced ICAP1 protein levels, although shICAP1-23 consistently resulted in greater loss of endogenous ICAP1. Unsurprisingly, GFP nuclear localization was unaffected by any of the shRNAs either visually or quantitatively (Fig. 9, *C* and *F*). Interestingly, in ICAP1 knockdown cells, KRIT1$_{FL}$ became more cytoplasmic (Fig. 9, *E* and *F*). Notably, this effect was most pronounced with shICAP1-23, which produced the greatest ICAP1 knockdown. Importantly, the ICAP1 binding-defective mutant GFP-KRIT1$_{FL/\not ICAP1}$ was less nuclear than GFP-KRIT1$_{FL}$ (Fig. 9, *E* and *F*) and was comparable with GFP-KRIT1$_{FL}$ in the absence of ICAP1 (Fig. 9*F*). Furthermore, the localization of GFP-KRIT1$_{FL/\not ICAP1}$ was not impacted by ICAP1 knockdown, and nuclear levels were comparable with GFP-KRIT$_{FL}$ in cells lacking ICAP1 (Fig. 9, *E* and *F*). Collectively, these data indicate that exogenous KRIT1 localization is affected by direct binding to endogenous ICAP1.

Discussion

ICAP1 has only two well validated binding partners: KRIT1 and integrin β1. Through the direct binding of its PTB domain to the cytoplasmic tail of integrin β1, ICAP1 represses β1 integ-

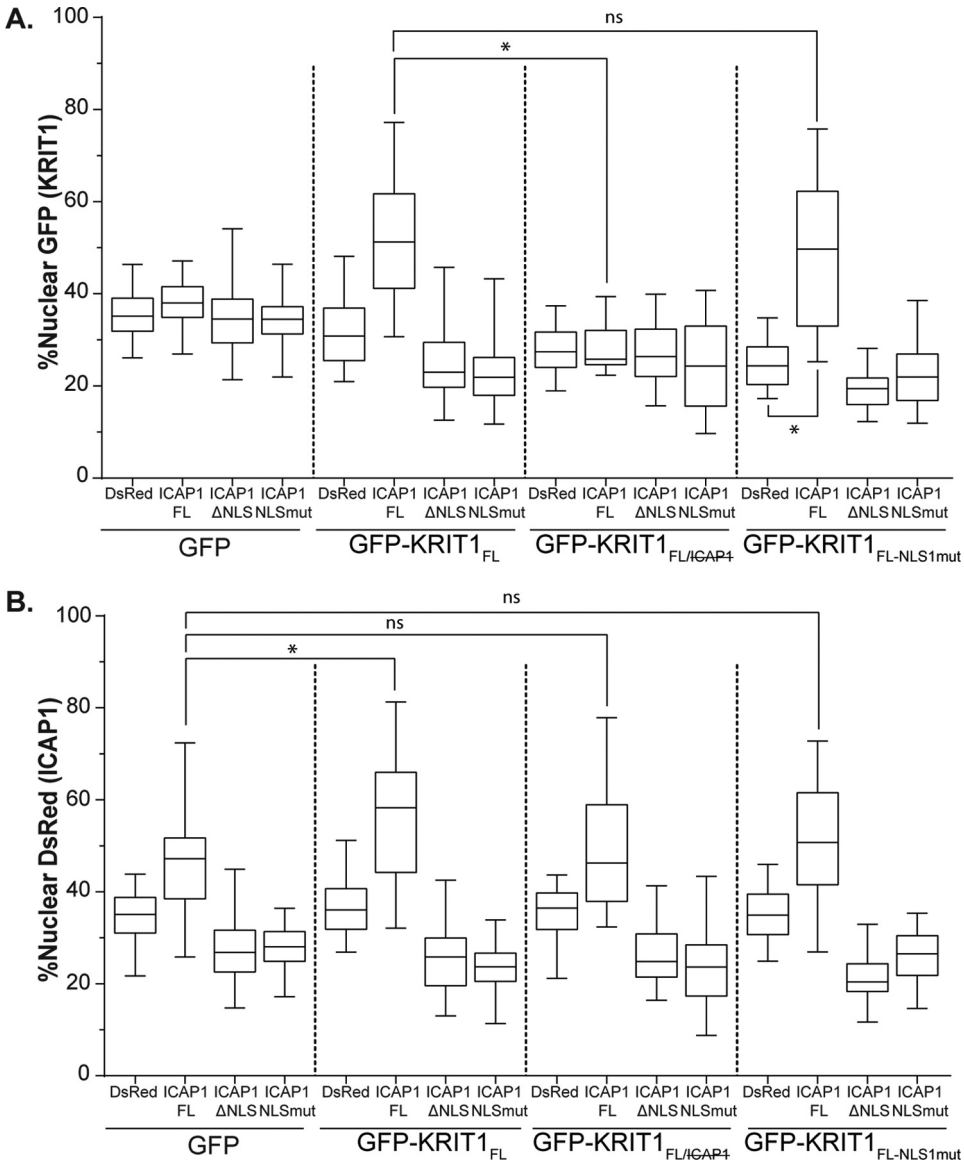

FIGURE 8. **Localization of KRIT1$_{FL}$ is driven by ICAP1.** CHO cells co-overexpressing GFP or GFP-tagged KRIT1 constructs and DsRed-tagged ICAP1 constructs were plated on fibronectin, fixed 24 h later, and stained with DAPI to identify nuclei. *A* and *B*, percentage nuclear fluorescence compared with the integrated fluorescence intensity of the entire cell for GFP (*A*) and DsRed (*B*) was calculated. *Boxes*, 25th through 50th and 50th through 75th percentile; *whiskers*, 5th through 95th percentile ($n = 47–103$ cells from three independent experiments). *, $p \leq 0.0001$ as determined by a one-way ANOVA with Tukey's correction for multiple tests.

rin activation and thus modulates downstream signaling (32–35). KRIT1 competes with β1 integrin for binding to ICAP1 and hence can reverse ICAP1-mediated integrin β1 repression (7). However, as KRIT1 protects ICAP1 from proteasomal degradation, it can also potentiate ICAP1-dependent processes (20), but impacts beyond the regulation of integrin β1 activation have not yet been determined. Here we investigated the control of ICAP1-mediated inhibition of integrin activation and found that nuclear localization of ICAP1 diminishes repression of integrin β1 activation. We further revealed that ICAP1 drives KRIT1 localization to the nucleus, suggesting that ICAP1 has important roles in determining KRIT1 subcellular localization.

ICAP1 Localization Affects Cellular Functions—Differential localization of signaling molecules is an important mechanism for regulation of signaling pathways. We demonstrate that ICAP1 contains a functional NLS, which is both necessary and sufficient for localization of ICAP1 to the nucleus. Nuclear accumulation reduces cytosolic ICAP1 levels, thereby diminishing the efficiency of ICAP1 repression of β1 integrin activation. Because integrin β1 is linked to a wide range of downstream signaling pathways, tight regulation is essential for proper cellular function. For example, increased β1 signaling leads to RhoA activation, and the RhoA activation and cell contractility seen upon the loss of KRIT1 or ICAP1 protein levels is dependent on integrin β1 (20, 47). Conversely, increased cytoplasmic ICAP1 leads to greater repression of integrin β1 activation, and thus general defects in cell adhesion and cell spreading would be expected. This could lead to a loss of endothelial cell polarity and lumen formation (48), phenotypes also seen in CCM patient samples (49). In addition to influencing levels of ICAP1 in the cytoplasm and thus impacting cytoplasmic functions of ICAP1, as discussed further below, nuclear localization

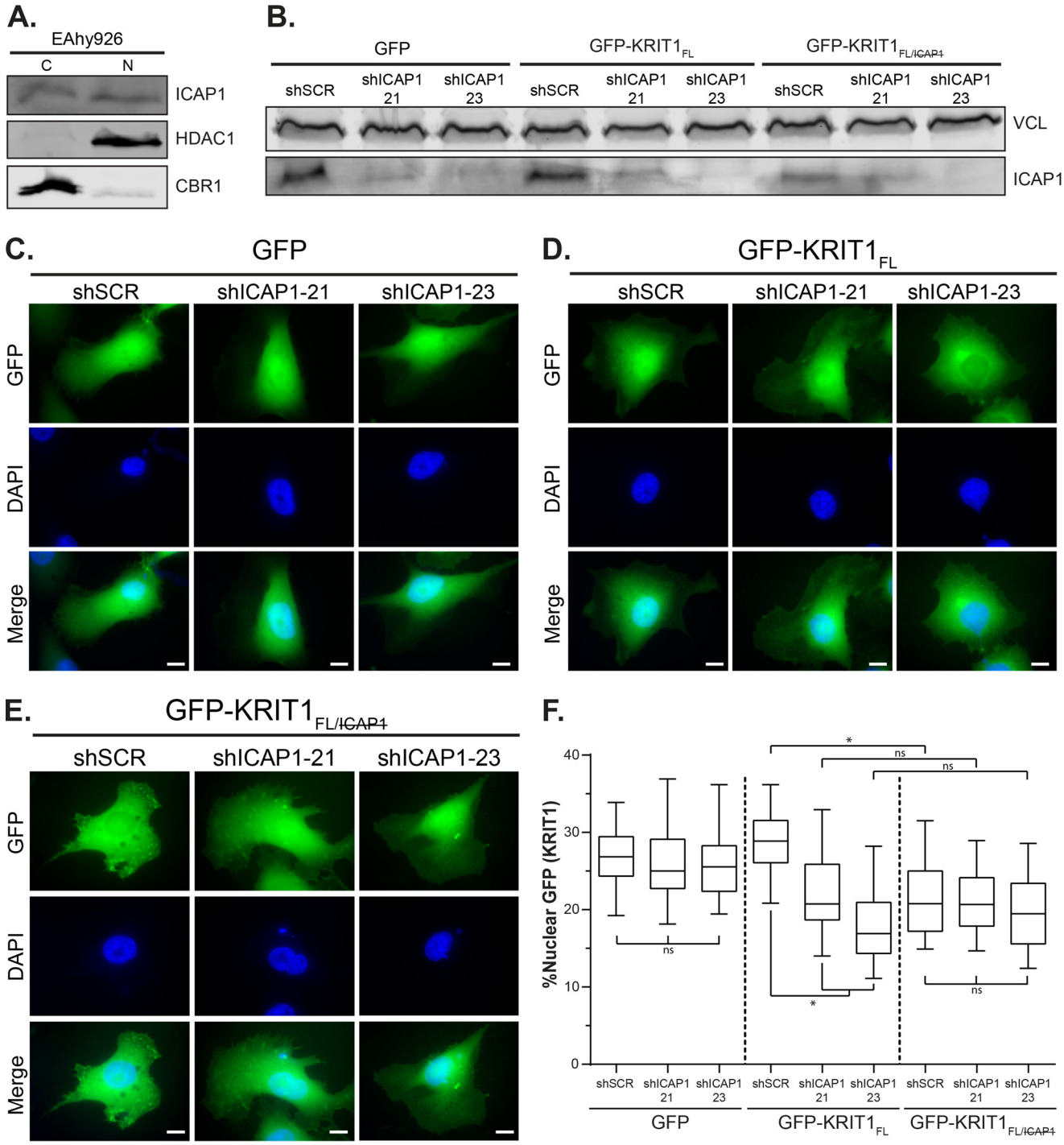

FIGURE 9. **Localization of exogenous KRIT1 in EAhy926 cells changes upon loss of ICAP1.** *A*, representative fractionation of endogenous ICAP1 in EAhy926 cells. *C*, 28% of the cytoplasmic fraction; *N*, 80% of the nuclear fraction. Carbonyl reductase (*CBR1*) and histone deacetylase (*HDAC1*) represent quality controls for cytoplasmic and nuclear fractions, respectively. Results are representative of three independent experiments. *B*, immunoblot of EAhy926 lysates that overexpress either GFP or GFP-tagged KRIT1 constructs and have been infected with either an shSCR or shRNAs targeting ICAP1 (shICAP1-21, shICAP1-23). Vinculin (*VCL*) was used as a loading control. *C–E*, EAhy926 cells infected with either shSCR or shICAP1 and overexpressing GFP or GFP-tagged KRIT1 constructs were plated on fibronectin, fixed 24 h later, and stained with DAPI to identify nuclei. Representative images are shown; *bar*, 10 μm. *F*, percentage of GFP intensity in the nucleus compared with the integrated GFP intensity of the entire cell. *Boxes*, 25th through 50th and 50th through 75th percentile; *whiskers*, 5th through 95th percentile ($n = 88–93$ cells from 3 independent experiments). *, $p \leq 0.0001$ as determined by a one-way ANOVA with Tukey's correction for multiple tests.

of ICAP1 may enhance nuclear roles of ICAP1. Thus, controlling subcellular localization permits switching between nuclear and cytoplasmic roles of ICAP1.

Signals that regulate ICAP1 nuclear localization are currently unknown but will be important subjects for future study. It will be interesting to inhibit the shuttling of endogenous ICAP1 and to determine the impact on integrin activation and integrin-mediated cellular processes, such as cell adhesion and migration. Unfortunately, we do not currently have sufficient information on the mechanisms or regulation of ICAP1 shut-

tling between the nucleus and the cytoplasm to experimentally disrupt it in a specific manner. For this reason, our current investigation of the effects of ICAP1 on KRIT1 localization and integrin activation has relied on overexpression of ICAP1 mutants with perturbed localization or on ICAP1 knockdown.

ICAP1 Drives the Localization of KRIT1—Our data demonstrate that the localization of ICAP1 strongly influences KRIT1 localization. Nuclear ICAP1 is capable of recruiting KRIT1 to the nucleus, even if the KRIT1 NLS is ablated. Furthermore, knockdown of endogenous ICAP1 reduces nuclear localization of exogenously expressed KRIT1. An important role of ICAP1 nuclear localization may therefore be the recruitment of KRIT1 to the nucleus. Consequently, it is likely that aberrant ICAP1 localization would lead to some KRIT1-related phenotypes. For example, the loss of KRIT1 leads to decreased β-catenin and VE-cadherin in cell-cell junctions, and this leads to increased nuclear β-catenin and the up-regulation of its transcriptional targets (26). Additionally, the loss of KRIT1 leads to the mislocalization of the polarity complex Tiam, Par3, and PKCζ and thus defects in directed migration and vascular lumen formation (49). It would be interesting to determine whether ICAP1-directed KRIT1 mislocalization would lead to similar phenotypes. We note that other KRIT1 binding partners also influence KRIT1 localization. In addition to shuttling between the nucleus and cytoplasm, KRIT1 also localizes to cell-cell junctions (22, 50, 51) and microtubules (52, 53). The KRIT1 FERM domain forms a ternary complex with membrane anchor protein HEG1 and Rap1, and KRIT1 mutants defective in binding to either HEG1 or Rap1 do not localize to cell-cell junctions (51, 54). The loss of CCM2 also leads to the loss of KRIT1 from cell-cell junctions, but it is unclear whether this is related to a direct interaction between the two proteins.

KRIT1 Influences the Localization of ICAP1—In addition to ICAP1 driving localization of KRIT1, our data demonstrate that, conversely, KRIT1 binding increases the levels of nuclear ICAP1 and that this effect is dependent on an intact KRIT1 NLS1. It is likely that although the ICAP1 NLS is sufficient to take both ICAP1 and KRIT1 into the nucleus, the KRIT1 NLS1 cooperates to allow increased nuclear import. Alternatively, KRIT1 NLS1 could decrease the nuclear export of the KRIT1-ICAP1 complex via an unknown mechanism.

Potential Roles for ICAP1-KRIT1 within the Nucleus—Neither the cellular stimulus that leads to a change in ICAP1-KRIT1 localization nor its functional significance has been determined. Our data support the hypothesis that nuclear retention of ICAP1 is a tool to modulate the cytoplasmic role of ICAP1 (suppression of β1 integrin activation), but ICAP1 may also have independent roles in the nucleus. The ICAP1 NLS has been implicated in the regulation of c-Myc mRNA expression (27), but it is currently unclear whether this is due to a specific nuclear role of ICAP1 or is secondary to changes in integrin β1 signaling. Our data suggest that one key role of nuclear ICAP1 could be to drive KRIT1 into the nucleus. KRIT1 expression has been linked to increased *SOD2* and *FOXO1* mRNA levels (25), although whether the nuclear localization of KRIT1 is required for the up-regulation is unknown. Intriguingly, one recent report demonstrated that KRIT1 localizes to actively transcribing regions of the nucleus (31), raising the possibility that KRIT1 has specific roles in the nucleus that would then be regulated by ICAP1 localization.

Potential Regulation of ICAP1-KRIT1 Localization—The balance between nuclear export and import determines the extent of nuclear accumulation. Changes in that equilibrium could dictate the different biological effects of either ICAP1 or KRIT1. The ICAP1 NLS lies within a predicted unstructured region N-terminal to the PTB domain. It is possible that a conformational change in ICAP1 or the direct binding of another protein could either expose or mask the NLS. Data indicating that the binding to integrin β1 leads to increased cytoplasmic ICAP1 potentially support this hypothesis (27). Additionally, phosphorylation has been shown to both enhance and suppress nuclear export (55). Because the ICAP1 NLS is just N-terminal to a serine/threonine-rich motif, this is another possible mechanism for ICAP1 localization regulation. Finally, whereas the ICAP1 NLS is sufficient to take KRIT1 into the nucleus even in the absence of the only functional KRIT1 NLS, KRIT1 increases ICAP1 nuclear localization, suggesting that the KRIT1 NLS may have a secondary role on both KRIT1 and KRIT1-ICAP1 complex localization, and this too may be regulated by additional binding partners, post-translational modifications, or conformational changes. In addition, although we saw no changes in nuclear localization when we mutated either the NES or the second NLS of KRIT1, it is possible that conformational changes and/or the binding of other partners would better expose or cooperate with these signals. There is evidence suggesting that KRIT1 may have both an "open" and a "closed" conformation due to head-tail interactions and that this affects subcellular localization (28, 52). Additionally, some reports suggest that the KRIT1/CCM2 interaction also influences KRIT1 localization (30), but it is still unclear how ICAP1 would affect this dynamic.

Implications for Understanding the CCM Disease—Mutations in one of the three CCM genes occurs in ~95% of familial CCM cases and ~67% of sporadic CCM cases with multiple lesions (56, 57). However, CCM gene mutations have been identified in only 5–20% of sporadic cases (58), despite familial and sporadic lesions being pathologically indistinguishable (15). One interesting possibility is that, in these lesions, CCM proteins are being functionally repressed, perhaps through mislocalization, yet the role and mechanism of CCM protein localization have not been extensively studied. Our work highlights the importance of KRIT1/ICAP1 interactions in determining subcellular localization of the complex, influencing cell adhesion and potentially additional functions.

Experimental Procedures

Antibodies/cDNA—Ligand-mimetic anti-αIIbβ3 PAC1 (BD Biosciences), anti-GFP (Rockland, catalogue no. 600-101-215), anti-ICAP-1 (R&D Systems, catalogue no. AF6805), anti-HDAC-1 (Santa Cruz Biotechnology, catalogue no. sc-7872), anti-carbonyl reductase (CBR1, Santa Cruz Biotechnology, Inc., catalogue no. sc-70212), and anti-vinculin (Sigma, V-9131) were purchased. The anti-ICAP-1 antibody was validated by knockdown. All other antibodies gave only bands of the expected size (or sizes) consistent with the manufacturers' validations. Wild-type and mutant ICAP1 and KRIT1 cDNAs pre-

viously used for protein expression/purification (7) were subcloned into pDsRed-C1 and pEGFP-C1 (Clontech). Additional mutations were introduced by QuikChange site-directed mutagenesis (Stratagene). Lentiviral ICAP1 and KRIT1 expression constructs were generated by the protocol of Fu *et al.* (61). In brief, attL1/attL2 sites were added to GFP-tagged cDNA by two rounds of PCR, and the final product, purified by agarose gel extraction, was used in a Gateway cloning reaction (Life Technologies) to insert the GFP-tagged construct into CMV-pLENTI-Hygro (Addgene). Lentiviral constructs in the pLKO vector (U6 promoter) containing shRNAs (target sequences in brackets) against ICAP1 (TRCN0000122921 [sequence 21, CCTGTGCAGAATTTCGAATAA] and TRCN0000122923 [sequence 23, TGAAGGGCCATTAGACCTGAT]), along with a scrambled control (TRC library-based lentiviral scramble; catalogue no. SHC002) were obtained from a TRC shRNA library (Sigma-Aldrich). All constructs used were authenticated by DNA sequencing.

Cell Culture—HEK 293T cells, CHO cells, and a previously described CHO cell line stably expressing chimeric αIIbα5β3β1 integrins (37) were cultured in Dulbecco's modified Eagle's medium containing 10% fetal bovine serum, 1% sodium pyruvate, and 1% nonessential amino acids (Gibco). EaHy926 cells were cultured in Dulbecco's modified Eagle's medium containing 10% fetal bovine serum, 1% sodium pyruvate, and 2% hypoxanthine-aminopterin-thymidine supplement (Gibco). Cells were regularly tested for the presence of mycoplasma using the MycoAlert^{TM} mycoplasma detection kit (Lonza).

Lentiviral Knockdown and Overexpression—Lentiviruses were produced by co-transfecting packaging vectors psPAX2 (viral proteins Gag and Rev under the SV40 promoter; Addgene plasmid 12260, a gift from D. Trono, École Polytechnique Fédérale de Lausanne, Lausanne, Switzerland) and pMD2.G (viral protein VSV-G expressed under the CMV promoter; Addgene plasmid 12259, a gift from D. Trono) into HEK 293T cells with the shRNA construct. Viral supernatant was collected 48 and 72 h after transfection and filtered with a 0.45-μm filter.

To establish polyclonal knockdown or overexpression lines, cells were incubated with viral supernatant and 8 μg/ml Polybrene for 18 h. Cells were either analyzed 48–72 h postinfection or selected with 2 μg/ml puromycin (pLKO) or 50 μg/ml hygromycin (CMV-pLENTI-Hygro) as appropriate.

Knockdown was assessed by immunoblotting of stable lines lysed in radioimmune precipitation assay buffer (50 mm Tris, pH 8.0, 150 mm NaCl, 1% Triton X-100, 0.5% sodium deoxycholate, and 0.1% SDS) containing cOmplete protease inhibitor mixture tablets (Roche Applied Science). Immunoblotting was performed with primary antibodies diluted in 5% milk in TBS-T (1:100 of α-ICAP1, 1:1000 of α-GFP, 1:10,000 of α-vinculin) fluorescent secondary antibodies (IR Dye800 or IR Dye680; LI-COR Biosciences; diluted 1:20,000 in 5% milk in TBS-T) and scanned on the Odyssey CLx infrared imaging system. Quantification was performed on the raw images in Image Studio (LI-COR Biosciences); lanes were defined, and bands were automatically identified. The profile feature was used to identify band boundaries, and lane background was subtracted. The signal for the protein of interest was normalized to that of the loading control. Optimization of images for publication was performed by adjusting the brightness and contrast in Image Studio (LI-COR Biosciences).

Integrin Activation Assays—The activation state of stably overexpressed αIIbα5β3β1 chimeric integrin in CHO cells transiently expressing GFP-tagged ICAP1 constructs was assessed in multicolor flow cytometry assays using a modification of methods described previously (36). CHO cells expressing chimeric αIIbα5β3β1 integrins were transfected with the indicated GFP expression constructs using linear polyethyleneimine, M_r 25,000 (Polysciences, Inc.) following the manufacturer's instructions. 24 h later, the cells were suspended and incubated with ligand-mimetic anti-αIIbβ3 monoclonal antibody IgM-PAC1 (BD Biosciences) in the presence or absence of 10 mM EDTA. Chimeric integrin expression was assessed in parallel by staining with anti-αIIbβ3 antibody D57 (59). Bound PAC1 and D57 were detected using Alexa 647 fluorophore-conjugated goat anti-mouse IgM and anti-mouse IgG (Invitrogen), respectively. The activation of endogenous α5β1 was assessed in CHO cells using methods described previously (36). Briefly, 5×10^5 cells were suspended and incubated with biotinylated GST-fibronectin type III repeats 9–11 (FN9–11) in the presence or absence of 10 mM EDTA. Integrin expression was assessed by parallel staining with PB1, an anti-α5 antibody (Developmental Studies Hybridoma Bank). Bound FN9–11 and PB1 were detected using allophycocyanin-conjugated streptavidin and Alexa-647 fluorophore-conjugated goat anti-mouse IgG (Invitrogen), respectively. Cells were analyzed on an LSRII flow cytometer (BD Biosciences), and data analysis was completed using FlowJo software. GFP-positive cells were gated such that the mean fluorescence intensities (MFIs) for GFP-positive cells were the same across all samples, ensuring that analysis was performed on populations expressing equivalent levels of exogenous protein. The activation index (AI) of cells gated to have equivalent mean GFP intensity was calculated as $AI = (F - F_0)/F_{integrin}$, where F is the geometric MFI of PAC1 or FN9–11 binding, F_0 is the MFI of PAC1 or FN9–11 binding in the presence of EDTA, and $F_{integrin}$ is the MFI of D57 or PB1 binding to transfected cells. To compare across experiments, data were expressed as the percentage of AI in the GFP-negative population within each sample. Data were charted, and statistical analyses were performed using GraphPad Prism.

His Tag-Integrin β Tail Pull-down Assays—GFP-tagged ICAP1 was expressed in CHO cells, and cells were lysed in 1 mM Na_3VO_4, 50 mM NaF, 40 mM $NaPP_i$, 50 mM NaCl, 150 mM sucrose, 10 mM Pipes, 0.5% Triton X-100, 0.1% deoxycholate, pH 6.8, and clarified by centrifugation. pGEX-6P-1 $ICAP1_{PTB}$ and $ICAP1_{FL}$ constructs were obtained as described previously (7). Both constructs were transformed in BL21 (DE3) Rosetta^{TM} (Novagen) cells and were cultivated at 37 °C to an A_{600} of 0.6. ICAP expression was induced by 0.1 mM isopropyl β-D-1-thiogalactopyranoside at 16 °C for 20 h. Cell pellets were then lysed in 50 mM Tris-HCl, pH 8.2, 100 mM NaCl, 5% glycerol, 0.2 mM tris(2-carboxyethyl) phosphine, and 1× cOmplete^{TM} EDTA free protease inhibitor mixture (Roche Applied Science). GST-ICAP was purified from the lysate on Sepharose-4B glutathione beads, and ICAP was eluted by incubation with recombinant 3C protease. Monomeric ICAP was further purified by size exclusion chromatography on a Superdex^{TM} S200

16/600pg column (GE Healthcare) in 50 mM Tris-HCl, pH 8.2, 100 mM NaCl, 5% glycerol, 0.1 mM tris(2-carboxyethyl) phosphine and concentrated using Amicon® Ultra-4 (Millipore) centrifugal filters. ICAP1 binding to purified recombinant His-tagged integrin tails was assessed in pull-down assays as described previously (36, 39).

Microscopy—Transfected cells were stained with CellTracker™ Deep Red Dye (Thermo Fisher Scientific) per the manufacturer's instructions. Cells were plated on coverslips coated with 10 μg/ml fibronectin (Sigma-Aldrich). 24 h after replating, cells were fixed in 4% paraformaldehyde in PBS, pH 7.4, for 30 min. Coverslips were washed with PBS and mounted using ProLong Diamond with 25 ng/ml DAPI added (Invitrogen). Images were acquired using a Nikon Eclipse Ti-S microscope with a $\times$100 objective using the μManager acquisition software (60). A minimum of 50 cells (from $\geq$3 replicates) were analyzed for each single-expression experiment, and a minimum of 75 cells (from $\geq$3 replicates) were analyzed for each double-expression experiment. We verified by immunoblot that exogenous proteins were of the expected size (data not shown).

Quantification of ICAP1-KRIT1 nuclear-cytoplasmic localization was performed using CellProfiler version 2.0 (40). Nuclear GFP and/or DsRed was quantified as the integrated intensity of the fluorophore within the nucleus, as defined by DAPI staining. The outer boundary of the cell was determined by the propagation method within CellProfiler version 2.0 using the CellTracker fluorescence signal (40). Data were charted, and statistical analyses were performed using GraphPad Prism.

Nuclear/Cytoplasmic Fractionation—Fractionation of cytoplasmic and nuclear proteins was performed using the NE-PER™ kit from Thermo Fisher Scientific following the manufacturer's instructions. 3×10^6 CHO cells or 2×10^6 EAhy.926 cells were used in each fractionation. After fractionation, cytoplasmic and nuclear fractions were each mixed with 4$\times$ Laemmli sample buffer and boiled for 5 min, and a fixed volume of each fraction was loaded onto 12 or 16% SDS-polyacrylamide gels. Separated proteins were transferred onto nitrocellulose or PVDF membranes, probed by immunoblotting with antibodies diluted in 5% milk in TBS-T (1:1000 of α-GFP, 1:1000 of α-HDAC1, 1:1000 of α-CBR1), and scanned with an Odyssey CLx infrared imaging system. For a given protein, the percentage of protein extracted from the nucleus was calculated by extrapolating the total amounts detected in cytoplasmic and nuclear fractions.

Author Contributions—K. M. D. and D. A. C. conceived and designed the research and prepared the manuscript. K. M. D. performed most experiments and data analyses. C. H.-C. performed the cellular fractionation assays seen in Figs. 3 (*C* and *D*) and 4 (*C* and *D*). B. S. performed the binding curve experiments seen in Fig. 2 (*C* and *D*). All authors reviewed the results and approved the final version of the manuscript.

Acknowledgments—We thank past and present members of the Calderwood laboratory and Titus Boggon for helpful insights and discussion.

References

1. Hynes, R. O. (2002) Integrins: bidirectional, allosteric signaling machines. *Cell* **110,** 673–687
2. Harburger, D. S., and Calderwood, D. A. (2009) Integrin signalling at a glance. *J. Cell Sci.* **122,** 159–163
3. Morse, E. M., Brahme, N. N., and Calderwood, D. A. (2014) Integrin cytoplasmic tail interactions. *Biochemistry* **53,** 810–820
4. Iwamoto, D. V., and Calderwood, D. A. (2015) Regulation of integrin-mediated adhesions. *Curr. Opin. Cell Biol.* **36,** 41–47
5. Calderwood, D. A., Campbell, I. D., and Critchley, D. R. (2013) Talins and kindlins: partners in integrin-mediated adhesion. *Nat. Rev. Mol. Cell Biol.* **14,** 503–517
6. Ye, F., Snider, A. K., and Ginsberg, M. H. (2014) Talin and kindlin: the one-two punch in integrin activation. *Front. Med.* **8,** 6–16
7. Liu, W., Draheim, K. M., Zhang, R., Calderwood, D. A., and Boggon, T. J. (2013) Mechanism for KRIT1 release of ICAP1-mediated suppression of integrin activation. *Mol. Cell* **49,** 719–729
8. Kiema, T., Lad, Y., Jiang, P., Oxley, C. L., Baldassarre, M., Wegener, K. L., Campbell, I. D., Ylänne, J., and Calderwood, D. A. (2006) The molecular basis of filamin binding to integrins and competition with talin. *Mol. Cell* **21,** 337–347
9. Millon-Frémillon, A., Bouvard, D., Grichine, A., Manet-Dupé, S., Block, M. R., and Albiges-Rizo, C. (2008) Cell adaptive response to extracellular matrix density is controlled by ICAP-1-dependent β1-integrin affinity. *J. Cell Biol.* **180,** 427–441
10. Zhang, J., Clatterbuck, R. E., Rigamonti, D., Chang, D. D., and Dietz, H. C. (2001) Interaction between krit1 and icap1α infers perturbation of integrin β1-mediated angiogenesis in the pathogenesis of cerebral cavernous malformation. *Hum. Mol. Genet.* **10,** 2953–2960
11. Zawistowski, J. S., Serebriiskii, I. G., Lee, M. F., Golemis, E. A., and Marchuk, D. A. (2002) KRIT1 association with the integrin-binding protein ICAP-1: a new direction in the elucidation of cerebral cavernous malformations (CCM1) pathogenesis. *Hum. Mol. Genet.* **11,** 389–396
12. Fisher, O. S., and Boggon, T. J. (2014) Signaling pathways and the cerebral cavernous malformations proteins: lessons from structural biology. *Cell Mol. Life Sci.* **71,** 1881–1892
13. Pozzati, E., Acciarri, N., Tognetti, F., Marliani, F., and Giangaspero, F. (1996) Growth, subsequent bleeding, and *de novo* appearance of cerebral cavernous angiomas. *Neurosurgery* **38,** 662–669; discussion 669–670
14. Rigamonti, D., Hadley, M. N., Drayer, B. P., Johnson, P. C., Hoenig-Rigamonti, K., Knight, J. T., and Spetzler, R. F. (1988) Cerebral cavernous malformations: incidence and familial occurrence. *N. Engl. J. Med.* **319,** 343–347
15. Tanriover, G., Sozen, B., Seker, A., Kilic, T., Gunel, M., and Demir, N. (2013) Ultrastructural analysis of vascular features in cerebral cavernous malformations. *Clin. Neurol. Neurosurg.* **115,** 438–444
16. Revencu, N., and Vikkula, M. (2006) Cerebral cavernous malformation: new molecular and clinical insights. *J. Med. Genet.* **43,** 716–721
17. Draheim, K. M., Fisher, O. S., Boggon, T. J., and Calderwood, D. A. (2014) Cerebral cavernous malformation proteins at a glance. *J. Cell Sci.* **127,** 701–707
18. Voss, K., Stahl, S., Schleider, E., Ullrich, S., Nickel, J., Mueller, T. D., and Felbor, U. (2007) CCM3 interacts with CCM2 indicating common pathogenesis for cerebral cavernous malformations. *Neurogenetics* **8,** 249–256
19. Stahl, S., Gaetzner, S., Voss, K., Brackertz, B., Schleider, E., Surucu, O., Kunze, E., Netzer, C., Korenke, C., Finckh, U., Habek, M., Poljakovic, Z., Elbracht, M., Rudnik-Schöneborn, S., Bertalanffy, H., *et al.* (2008) Novel CCM1, CCM2, and CCM3 mutations in patients with cerebral cavernous malformations: in-frame deletion in CCM2 prevents formation of a CCM1/CCM2/CCM3 protein complex. *Hum. Mutat.* **29,** 709–717
20. Faurobert, E., Rome, C., Lisowska, J., Manet-Dupé, S., Boulday, G., Malbouyres, M., Balland, M., Bouin, A. P., Kéramidas, M., Bouvard, D., Coll, J. L., Ruggiero, F., Tournier-Lasserve, E., and Albiges-Rizo, C. (2013)

CCM1-ICAP-1 complex controls β1 integrin-dependent endothelial contractility and fibronectin remodeling. *J. Cell Biol.* **202,** 545–561
21. Borikova, A. L., Dibble, C. F., Sciaky, N., Welch, C. M., Abell, A. N., Bencharit, S., and Johnson, G. L. (2010) Rho kinase inhibition rescues the endothelial cell cerebral cavernous malformation phenotype. *J. Biol. Chem.* **285,** 11760–11764
22. Stockton, R. A., Shenkar, R., Awad, I. A., and Ginsberg, M. H. (2010) Cerebral cavernous malformations proteins inhibit Rho kinase to stabilize vascular integrity. *J. Exp. Med.* **207,** 881–896
23. Whitehead, K. J., Chan, A. C., Navankasattusas, S., Koh, W., London, N. R., Ling, J., Mayo, A. H., Drakos, S. G., Jones, C. A., Zhu, W., Marchuk, D. A., Davis, G. E., and Li, D. Y. (2009) The cerebral cavernous malformation signaling pathway promotes vascular integrity via Rho GTPases. *Nat. Med.* **15,** 177–184
24. Wüstehube, J., Bartol, A., Liebler, S. S., Brütsch, R., Zhu, Y., Felbor, U., Sure, U., Augustin, H. G., and Fischer, A. (2010) Cerebral cavernous malformation protein CCM1 inhibits sprouting angiogenesis by activating DELTA-NOTCH signaling. *Proc. Natl. Acad. Sci. U.S.A.* **107,** 12640–12645
25. Goitre, L., Balzac, F., Degani, S., Degan, P., Marchi, S., Pinton, P., and Retta, S. F. (2010) KRIT1 regulates the homeostasis of intracellular reactive oxygen species. *PLoS One* **5,** e11786
26. Glading, A. J., and Ginsberg, M. H. (2010) Rap1 and its effector KRIT1/CCM1 regulate β-catenin signaling. *Dis. Model. Mech.* **3,** 73–83
27. Fournier, H. N., Dupé-Manet, S., Bouvard, D., Luton, F., Degani, S., Block, M. R., Retta, S. F., and Albiges-Rizo, C. (2005) Nuclear translocation of integrin cytoplasmic domain-associated protein 1 stimulates cellular proliferation. *Mol. Biol. Cell* **16,** 1859–1871
28. Francalanci, F., Avolio, M., De Luca, E., Longo, D., Menchise, V., Guazzi, P., Sgrò, F., Marino, M., Goitre, L., Balzac, F., Trabalzini, L., and Retta, S. F. (2009) Structural and functional differences between KRIT1A and KRIT1B isoforms: a framework for understanding CCM pathogenesis. *Exp. Cell Res.* **315,** 285–303
29. Bouvard, D., Millon-Fremillon, A., Dupe-Manet, S., Block, M. R., and Albiges-Rizo, C. (2006) Unraveling ICAP-1 function: toward a new direction? *Eur. J. Cell Biol.* **85,** 275–282
30. Zawistowski, J. S., Stalheim, L., Uhlik, M. T., Abell, A. N., Ancrile, B. B., Johnson, G. L., and Marchuk, D. A. (2005) CCM1 and CCM2 protein interactions in cell signaling: implications for cerebral cavernous malformations pathogenesis. *Hum. Mol. Genet.* **14,** 2521–2531
31. Marzo, S., Galimberti, V., and Biggiogera, M. (2014) Unexpected distribution of KRIT1 inside the nucleus: new insight in a complex molecular pathway. *Eur. J. Histochem.* **58,** 2358
32. Bouvard, D., Aszodi, A., Kostka, G., Block, M. R., Albigès-Rizo, C., and Fässler, R. (2007) Defective osteoblast function in ICAP-1-deficient mice. *Development* **134,** 2615–2625
33. Bouvard, D., Vignoud, L., Dupé-Manet, S., Abed, N., Fournier, H. N., Vincent-Monegat, C., Retta, S. F., Fassler, R., and Block, M. R. (2003) Disruption of focal adhesions by integrin cytoplasmic domain-associated protein-1 α. *J. Biol. Chem.* **278,** 6567–6574
34. Brunner, M., Millon-Frémillon, A., Chevalier, G., Nakchbandi, I. A., Mosher, D., Block, M. R., Albigès-Rizo, C., and Bouvard, D. (2011) Osteoblast mineralization requires beta1 integrin/ICAP-1-dependent fibronectin deposition. *J. Cell Biol.* **194,** 307–322
35. Liu, W., and Boggon, T. J. (2013) Cocrystal structure of the ICAP1 PTB domain in complex with a KRIT1 peptide. *Acta Crystallogr. Sect. F Struct. Biol. Cryst. Commun.* **69,** 494–498
36. Bouaouina, M., Harburger, D. S., and Calderwood, D. A. (2012) Talin and signaling through integrins. *Methods Mol. Biol.* **757,** 325–347
37. O'Toole, T. E., Katagiri, Y., Faull, R. J., Peter, K., Tamura, R., Quaranta, V., Loftus, J. C., Shattil, S. J., and Ginsberg, M. H. (1994) Integrin cytoplasmic domains mediate inside-out signal transduction. *J. Cell Biol.* **124,** 1047–1059
38. Millon-Frémillon, A., Brunner, M., Abed, N., Collomb, E., Ribba, A. S., Block, M. R., Albigès-Rizo, C., and Bouvard, D. (2013) Calcium and calmodulin-dependent serine/threonine protein kinase type II (CaMKII)-mediated intramolecular opening of integrin cytoplasmic domain-associated protein-1 (ICAP-1α) negatively regulates β1 integrins. *J. Biol. Chem.* **288,** 20248–20260
39. Lad, Y., Harburger, D. S., and Calderwood, D. A. (2007) Integrin cytoskeletal interactions. *Methods Enzymol.* **426,** 69–84
40. Carpenter, A. E., Jones, T. R., Lamprecht, M. R., Clarke, C., Kang, I. H., Friman, O., Guertin, D. A., Chang, J. H., Lindquist, R. A., Moffat, J., Golland, P., and Sabatini, D. M. (2006) CellProfiler: image analysis software for identifying and quantifying cell phenotypes. *Genome Biol.* **7,** R100
41. Tu, X., Batta, P., Innocent, N., Prisco, M., Casaburi, I., Belletti, B., and Baserga, R. (2002) Nuclear translocation of insulin receptor substrate-1 by oncogenes and Igf-I: effect on ribosomal RNA synthesis. *J. Biol. Chem.* **277,** 44357–44365
42. Shaiken, T. E., and Opekun, A. R. (2014) Dissecting the cell to nucleus, perinucleus and cytosol. *Sci. Rep.* **4,** 4923
43. Zhang, J., Basu, S., Rigamonti, D., Dietz, H. C., and Clatterbuck, R. E. (2008) Krit1 modulates β1-integrin-mediated endothelial cell proliferation. *Neurosurgery* **63,** 571–578; discussion 578
44. Zhang, J., Rigamonti, D., Dietz, H. C., and Clatterbuck, R. E. (2007) Interaction between krit1 and malcavernin: implications for the pathogenesis of cerebral cavernous malformations. *Neurosurgery* **60,** 353–359; discussion 359
45. Baycin-Hizal, D., Tabb, D. L., Chaerkady, R., Chen, L., Lewis, N. E., Nagarajan, H., Sarkaria, V., Kumar, A., Wolozny, D., Colao, J., Jacobson, E., Tian, Y., O'Meally, R. N., Krag, S. S., Cole, R. N., *et al.* (2012) Proteomic analysis of Chinese hamster ovary cells. *J. Proteome Res.* **11,** 5265–5276
46. Bouïs, D., Hospers, G. A., Meijer, C., Molema, G., and Mulder, N. H. (2001) Endothelium *in vitro*: a review of human vascular endothelial cell lines for blood vessel-related research. *Angiogenesis* **4,** 91–102
47. Huveneers, S., Truong, H., Fässler, R., Sonnenberg, A., and Danen, E. H. (2008) Binding of soluble fibronectin to integrin α5 β1: link to focal adhesion redistribution and contractile shape. *J. Cell Sci.* **121,** 2452–2462
48. Zovein, A. C., Luque, A., Turlo, K. A., Hofmann, J. J., Yee, K. M., Becker, M. S., Fassler, R., Mellman, I., Lane, T. F., and Iruela-Arispe, M. L. (2010) β1 integrin establishes endothelial cell polarity and arteriolar lumen formation via a Par3-dependent mechanism. *Dev. Cell* **18,** 39–51
49. Lampugnani, M. G., Orsenigo, F., Rudini, N., Maddaluno, L., Boulday, G., Chapon, F., and Dejana, E. (2010) CCM1 regulates vascular-lumen organization by inducing endothelial polarity. *J. Cell Sci.* **123,** 1073–1080
50. Glading, A., Han, J., Stockton, R. A., and Ginsberg, M. H. (2007) KRIT-1/CCM1 is a Rap1 effector that regulates endothelial cell cell junctions. *J. Cell Biol.* **179,** 247–254
51. Gingras, A. R., Liu, J. J., and Ginsberg, M. H. (2012) Structural basis of the junctional anchorage of the cerebral cavernous malformations complex. *J. Cell Biol.* **199,** 39–48
52. Béraud-Dufour, S., Gautier, R., Albiges-Rizo, C., Chardin, P., and Faurobert, E. (2007) Krit 1 interactions with microtubules and membranes are regulated by Rap1 and integrin cytoplasmic domain associated protein-1. *FEBS J.* **274,** 5518–5532
53. Gunel, M., Laurans, M. S., Shin, D., DiLuna, M. L., Voorhees, J., Choate, K., Nelson-Williams, C., and Lifton, R. P. (2002) KRIT1, a gene mutated in cerebral cavernous malformation, encodes a microtubule-associated protein. *Proc. Natl. Acad. Sci. U.S.A.* **99,** 10677–10682
54. Gingras, A. R., Puzon-McLaughlin, W., and Ginsberg, M. H. (2013) The structure of the ternary complex of Krev interaction trapped 1 (KRIT1) bound to both the Rap1 GTPase and the heart of glass (HEG1) cytoplasmic tail. *J. Biol. Chem.* **288,** 23639–23649
55. Nardozzi, J. D., Lott, K., and Cingolani, G. (2010) Phosphorylation meets nuclear import: a review. *Cell Commun. Signal.* **8,** 32
56. Cavalcanti, D. D., Kalani, M. Y., Martirosyan, N. L., Eales, J., Spetzler, R. F., and Preul, M. C. (2012) Cerebral cavernous malformations: from genes to proteins to disease. *J. Neurosurg.* **116,** 122–132
57. Riant, F., Cecillon, M., Saugier-Veber, P., and Tournier-Lasserve, E. (2013) CCM molecular screening in a diagnosis context: novel unclassified vari-

ants leading to abnormal splicing and importance of large deletions. *Neurogenetics* **14,** 133–141

58. McDonald, D. A., Shi, C., Shenkar, R., Gallione, C. J., Akers, A. L., Li, S., De Castro, N., Berg, M. J., Corcoran, D. L., Awad, I. A., and Marchuk, D. A. (2014) Lesions from patients with sporadic cerebral cavernous malformations harbor somatic mutations in the CCM genes: evidence for a common biochemical pathway for CCM pathogenesis. *Hum. Mol. Genet.* **23,** 4357–4370
59. Tozer, E. C., Liddington, R. C., Sutcliffe, M. J., Smeeton, A. H., and Loftus, J. C. (1996) Ligand binding to integrin αIIbβ3 is dependent on a MIDAS-like domain in the β3 subunit. *J. Biol. Chem.* **271,** 21978–21984
60. Edelstein, A., Amodaj, N., Hoover, K., Vale, R., and Stuurman, N. (2010) Computer control of microscopes using microManager. *Curr. Protoc. Mol. Biol.* 10.1002/0471142727.mb1420s92
61. Fu, C., Wehr, D. R., Edwards, J., and Hauge, B. (2008) Rapid one-step recombinational cloning. *Nucleic Acids Res.* **36,** e54